RSC Advances

PAPER

View Article Online
View Journal | View Issue

Cite this: *RSC Adv.*, 2023, **13**, 17398

The unusual effect of paraffin wax on the thermal decomposition of cyclotetramethylenetetranitramine†

Zunjian Hu,[ab] Wei Peng,[ab] Gang Li,[a] Qian Yu,[a] Fang Yang,[a] Zhirong Suo,*[b] Ruijuan Xu*[a] and Chuande Zhao*[a]

Received 28th February 2023
Accepted 24th March 2023

DOI: 10.1039/d3ra01360j

rsc.li/rsc-advances

The practical application of paraffin wax (PW) in cyclotetramethylenetetranitramine (HMX)-based polymer-bonded explosive (PBX) requires an understanding of its effect on the thermal decomposition of HMX. In this work, by comparing the thermal decomposition of HMX and a HMX/PW mixture, combined with crystal morphology analysis, molecular dynamics simulation, kinetic analysis, and gas product analysis, the unusual phenomenon and mechanism of the PW effect on the thermal decomposition of HMX were evaluated. During the initial decomposition, PW infiltrates the crystal surface of HMX, reduces the energy barrier for chemical bond dissociation, and induces the decomposition of molecules on HMX crystals, resulting in a lower initial decomposition temperature. PW consumes the active gas produced by HMX with further thermal decomposition and inhibits the dramatic increase of the HMX thermal decomposition rate. In decomposition kinetics, this effect is manifested as PW inhibits transition from an *n*-order reaction to an autocatalytic reaction.

1. Introduction

Polymer-bonded explosive (PBX), a typical composite material formed by pure explosives, binder, desensitizer, stabilizer, and other components, is widely used in aerospace and military fields.[1–3] However, their comprehensive design and regulation basis have not been formed in nearly one hundred years. The reason for this is the nature of the PBX and some aspects of working with explosives (licensing, safety requirements, *etc.*).[4,5] The relationship between PBX components is complex. Mastering the effects of various additive components on pure explosives can promote PBX development.[6–9]

Cyclotetramethylenetetranitramine (HMX) is a typical high-energy pure explosive with a detonation velocity of up to 9.2 km s^{-1}; however, it suffers from high sensitivity (impact sensitivity H_{50} is between 28 and 32 cm).[10,11] Experimental and theoretical studies reveal that if paraffin wax (PW), an amorphous mixture of long-chained alkanes, is coated on the surface of HMX crystals, the shear stress intensity is reduced, making the crystals slip more easily under external mechanical forces. This slip disperses the mechanical forces, causing HMX less prone to decompose and ignition, reducing mechanical sensitivity.[12–14] However, to further promote PW's application as an additive in HMX-based PBX, the influence of PW on the thermal decomposition of HMX must be evaluated, which is of great significance for evaluating the thermal safety of HMX-based PBX. Unfortunately, the effect of PW on the thermal decomposition of HMX has not been reported yet. A few reports on other additive components in PBX affecting the decomposition of HMX have been published.[15–17] It is believed that additives accept H from HMX's main ring or donate H to the nitro group in HMX, inducing ring opening or nitro dissociation-induced thermal decomposition. However, this mechanism cannot explain the effect of PW on HMX's thermal decomposition temperature since PW lacks H-accepting or donating groups.

In this work, the effect of PW on HMX's thermal decomposition was studied. PW can infiltrate the surface of HMX crystals, reduce the chemical bond dissociation energy barrier, induce the decomposition of molecules on HMX crystals' surface, and reduce the initial decomposition temperature. Under further thermal decomposition, PW consumes the active gas produced by HMX decomposition and inhibits the dramatic increase of the thermal decomposition rate. Meanwhile, the kinetic analysis showed that PW inhibited the transition from an *n*-order reaction to an autocatalytic reaction as the reaction proceeded. The ability of PW to induce HMX decomposition and inhibit the rapid increase of the decomposition rate indicates that PW plays a positive role in improving the thermal safety of HMX-based PBX.

[a]*Institute of Chemical Materials, China Academy of Engineering Physics (CAEP), Mianyang, Sichuan 621900, China. E-mail: xuruij@caep.cn; c.d.zhao@caep.cn*

[b]*School of Materials Science and Engineering, Southwest University of Science and Technology, Mianyang 621010, China. E-mail: suozhirong@163.com*

† Electronic supplementary information (ESI) available. See DOI: https://doi.org/10.1039/d3ra01360j

2. Experimental section

2.1 Sample

HMX is produced by Gansu Baiyin Chemical Co., Ltd, with an average particle size of 250.0 μm. PW is a white powder at room temperature provided by the Shanghai Institute of Organic Chemistry, Chinese Academy of Sciences.

2.2 Thermal decomposition experiment

In order to better understand the decomposition process of the PW/HMX mixture, thermal decomposition experiments of PW/HMX and HMX were carried out, and PW and HMX were directly mixed at room temperature with a 1 : 1 mass ratio. The weight of the PW and HMX samples was around 1.2 mg. The thermal decomposition experiments were carried out using a TG-DSC (Q200 TA company, USA) instrument with an open-hole aluminum crucible. The heating program was 10 K min^{-1} from room temperature to 343 K and then to 623 K at 1 K min^{-1}. All the experiments were carried out in a nitrogen atmosphere at a flow rate of 30 mL min^{-1}.

2.3 Morphology observation experiment

Hot table micro-morphology observation experiments of the PW/HMX mixture and HMX were performed using a Linkam LTS420 hot table for heating and cooling. The *in situ* observations were carried out on an open hot table using an optical microscope (SCOPE.A1, ZEISS). The heating program was 10 K min^{-1} from room temperature to 393 K and then 1 K min^{-1} to 473 K. The samples at different temperatures were prepared using TG-DSC and were observed under a scanning electron microscope (ZEISS) after cooling to room temperature.

2.4 Surface molecular structure characterization experiments

The surface structures of the PW/HMX mixture and HMX at different temperatures were characterized using a micro-laser Raman (Renishaw) with a 532 nm wavelength. The samples were prepared in a TG-DSC calorimeter.

2.5 Online analysis of gas products

The online gas decomposition product was carried out using an adiabatic acceleration rate calorimeter (ARC,phi-TECII)-gas chromatography-mass spectrometer (GC-MS, Agilent 7890B-5977A MSD) combined system. The adiabatic acceleration calorimeter used helium as the carrier gas, the gas flow rate was 20 mL min^{-1}, and the heating program was the same as described in Section 2.6. Gas chromatography-mass spectrometry (GC-MS) conditions were as follows: Haysep N column, Mol sieve 13x column, porapak Q column, and helium as the carrier gas.

2.6 Decomposition experiment under adiabatic conditions

The self-sustaining decomposition behavior of PW/HMX (161.15 mg/161.09 mg) and HMX (161.12 mg) under adiabatic conditions was studied using the adiabatic acceleration calorimeter (TAC-500A, Young instruments). The sample was placed in a 1/4-inch stainless steel bomb with a thermocouple at the top of the bomb, sealed with an air atmosphere, initially heated to 373 K, and then equilibrated for 60 min, followed by a 40 min seek for an exothermic signal, which could be detected if the self-heat rate (SHR) was over 0.02 K min^{-1}. Then, the temperature was increased by 3 K with repeated heat–wait–seek (H–W–S) periods until the exothermic signal was detected. This H–W–S mode was continued till the end of sample decomposition.

2.7 Computational method

The PW/HMX and HMX system was subjected to molecular dynamics simulations with the ReaxFF reactive force field in the *NVT* ensemble for 150 ps at the temperature of 900 K using the open-source package LAMMPS.[18] Here, a relatively high temperature accommodates the chemical reactions within a reasonable simulation time. This strategy is reactive MD simulations favoured to accelerate chemical reactions, and it has been shown that the high temperatures may not affect initiation reaction mechanisms.[19,20] The simulated PW/HMX and HMX system temperature was controlled using a Nose–Hoover thermostat, and the integration time step was set to 0.1 fs to ensure the correct dynamics at high temperatures.

3. Results and discussion

3.1 Thermal decomposition behaviour

The DSC curves of the HMX and PW/HMX mixture obtained at a heating rate of 1 K min^{-1} are shown in Fig. 1. HMX begins to decompose at 519 K, the peak temperature is at 543 K, and there is an endothermic peak at 455 K corresponding to the β–δ phase transition. The DSC curve of the PW/HMX mixture demonstrates two decomposition processes. The first one begins at 420 K, and the endothermic peak of HMX corresponds to the β–

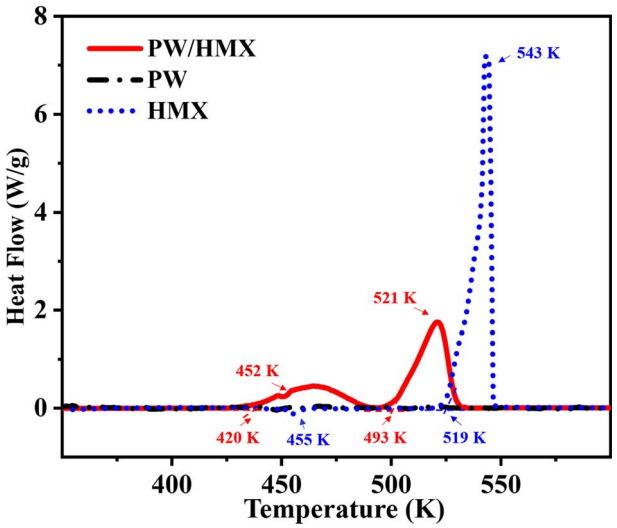

Fig. 1 DSC curves of HMX, PW and PW/HMX mixture obtained at a heating rate of 1 K min^{-1} and N_2 flow rate of 30 mL min^{-1}.

δ phase transition that appears at 452 K. No change relative to the phase transition temperature of HMX can be observed. Then, the second process begins, during which the initial decomposition temperature decreases from 519 K to 493 K, while the peak temperature decreases from 543 K to 521 K. Compared with HMX, the initial temperatures of the two exothermic peaks of the PW/HMX mixture decreased significantly. Since PW does not exothermic before 573 K, this indicates that the PW could induce a small amount of HMX and cause the remaining HMX to decompose earlier.

3.2 Structural and morphological changes during the first decomposition of PW/HMX

To investigate the morphology changes in the microstructure of PW/HMX mixtures during the first decomposition process, we used an *in situ* hot table optical microscope. The melting point of PW is 363 K. Before the first decomposition of PW/HMX starts, the mixture is first transformed from a solid/solid state to a solid/liquid state. It can be seen in Fig. 2 that between 423 and 433 K, a small number of bubbles form on the surface of the HMX crystal, which then diffuse into the liquid PW. When the temperature reaches 453 K, the light transmittance of the HMX crystal in the mixture begins to decrease, which becomes much more prominent at 458 K. Optical microscopy images of HMX taken in the 433–467 K range are shown in Fig. S1.† The appearance and light transmittance of the HMX crystal does not show obvious changes. This indicates that the change in the light transmittance of the HMX crystal within PW/HMX is mainly related to the decomposition of HMX.

The morphology of PW/HMX following the first decomposition process was investigated by scanning electron microscopy. Both HMX and PW/HMX samples were prepared in DSC, and quickly taken out and cooled in liquid nitrogen. It can be seen in Fig. 3 that during the first decomposition of the mixture, HMX is completely embedded in PW. By the end of this process, the surface of PW became porous due to the released gases originating from the decomposition of HMX. At the same temperature, cracks appeared on the surface of the HMX crystal due to phase transition, but no decomposition occurred.

Changes in the molecular structure of HMX and PW/HMX during the first decomposition process were investigated by Raman spectroscopy (Fig. 4). For HMX, due to the β–δ phase transition,[21] the absorption bands at 3038 cm^{-1}, 3029 cm^{-1}, and 2994 cm^{-1}, corresponding to asymmetric stretching and symmetrical stretching vibrations of CH_2, gradually weaken with increasing temperature. When the temperature reaches 463 K, the crystallinity decreases due to molecular rotations on the surface of HMX, and the absorption band intensity also decreases significantly.[22] After mixing PW with HMX, the absorption band at 2994 cm^{-1}, corresponding to CH_2 symmetrical stretching vibrations in HMX, blue-shifts with the increase in temperature. This indicates that PW molecules interact with molecules on the surface of HMX. When the temperature reaches 453 K, the absorption intensity of C–H stretching vibrations in PW at 2875 cm^{-1} is significantly greater than that of each characteristic peak in HMX. This means that the interaction between PW molecules and HMX surface molecules is further enhanced.

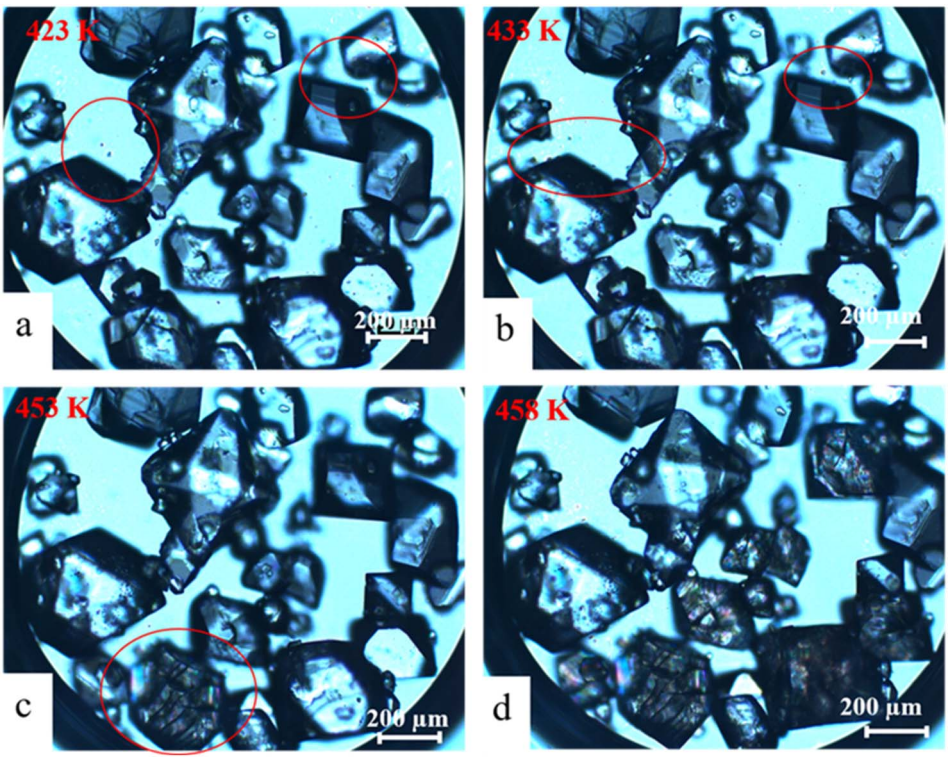

Fig. 2 Micrographs of PW/HMX observed with an *in situ* optical microscope.

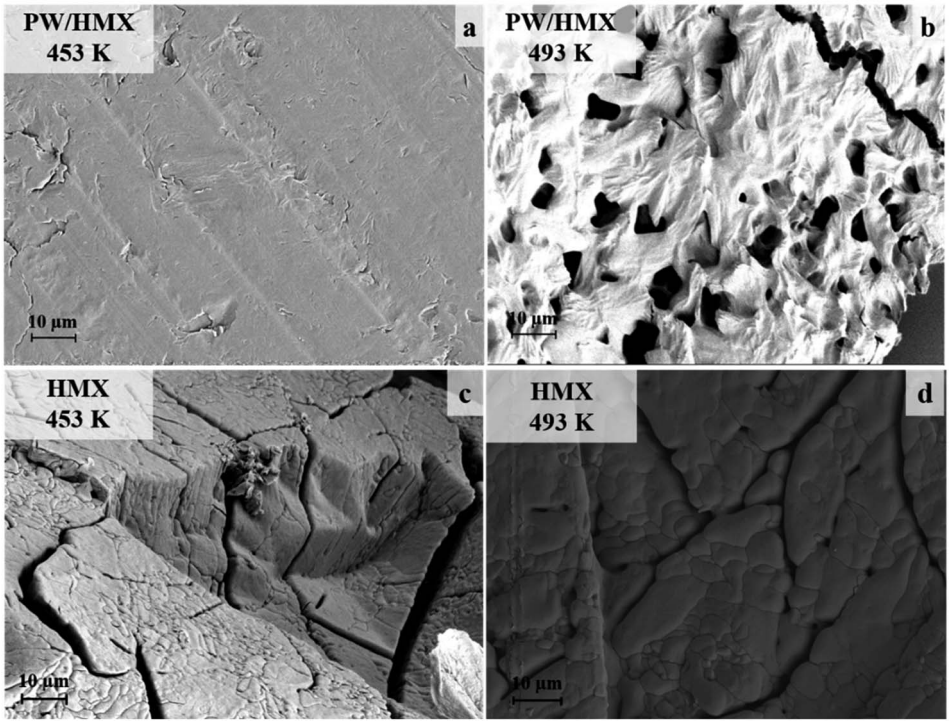

Fig. 3 SEM images of HMX and PW/HMX after heat treatment at different temperatures.

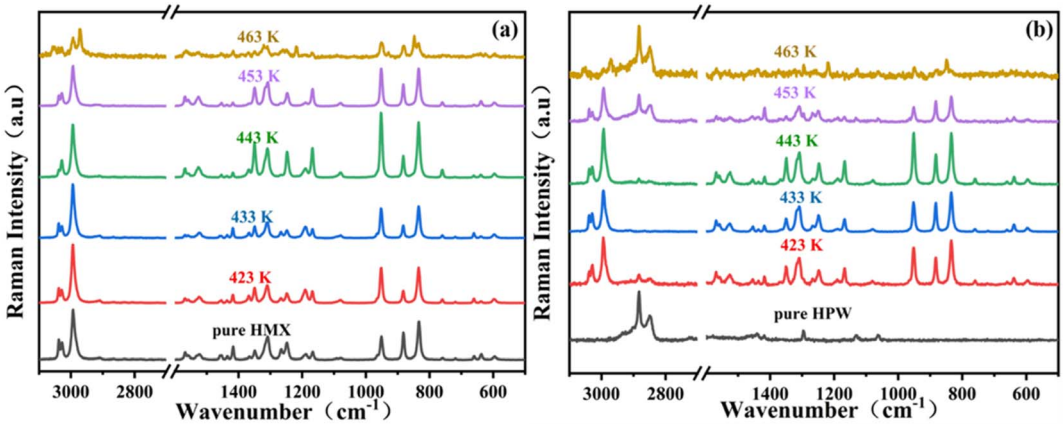

Fig. 4 Raman spectra of (a) HMX and (b) PW/HMX recorded following heat treatment at different temperatures.

To understand the effect of PW on the initial decomposition of the HMX crystal, we carried out simulations with the LAMMPS software to simulate the initial decomposition process at 900 K. For this purpose, β-HMX crystals of 5 nm (Fig. 5a), and β-HMX crystals embedded in either a small amount (Fig. 5b) or a large amount of PW (Fig. 5c) were used. Based on Fig. 5a, a small number of β-HMX molecules were separated from the β-HMX crystal in 20 ps, and this number increased to significantly over 150 ps. In Fig. 5b, the β-HMX molecules on the crystal surface detached at 2 and 6 ps. When a large amount of PW was embedded in the β-HMX crystals, the β-HMX molecules on the surface detach at 4 ps (Fig. 5c). Based on the simulation results, the decomposition of β-HMX crystals induced by PW mainly starts at the surface under thermal stimulation. The binding of the lattice to the surface molecules of the HMX crystal is weak, so the N–NO_2 bond dissociation energy and HONO elimination reaction energy are lower than 25.1 kJ mol^{-1} and 54.4 kJ mol^{-1},[23] respectively. This also shows that HMX surface molecules are easier to decompose.

The surface energy of the samples was also investigated (Table S1†). The contact angles between HMX/water and PW/water were 132°[24] and 139°, respectively (Fig. S2†). It can be seen that the polarity of HMX and PW are similar, and there is a remarkable difference in their surface energies (Table S2†). This indicates that PW can easily coat the surface of HMX and penetrate it. This effect changes the molecular state on the

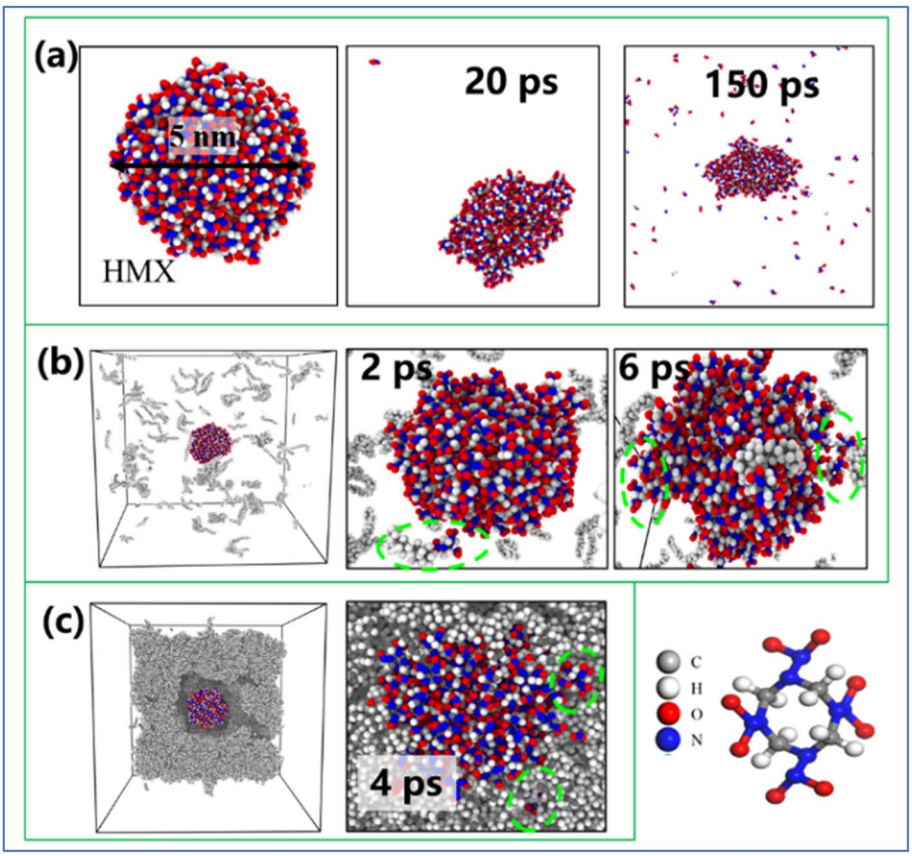

Fig. 5 Decomposition of (a) HMX, (b) mixture, and (c) mixture under ideal conditions at a constant temperature of 900 K.

surface of the HMX crystal and induces its decomposition. Additionally, the decomposition of PW takes a long time, which plays a significant role in the whole HMX decomposition process. This results in an increasing number of crystal defects on the surface of HMX in PW/HMX. The crystal defects that are easy to decompose in HMX lead to the advancement of the second decomposition process of PW/HMX.

3.3 Adiabatic decomposition and kinetics

The slow cook-off performance is an essential parameter for assessing the thermal safety of explosives. During a slow cook-off, heat accumulates from the decomposition of pure explosives as the temperature increases. This can result in combustion or the explosion of PBX as the chemical energy is released. Less released energy means lower reaction intensity and better slow cook-off performance and *vice versa*.[25–27] Recent experiments reported that the more gas generated by decomposition before thermal runaway, the greater the pre-damage caused and the lower the reaction intensity of slow cook-off.[28–31] Since the explosives rapidly combust and explode after entering from thermal decomposition to thermal runaway, the thermal pre-damage before this significantly influences the intensity of the reaction. Therefore, we used an adiabatic reaction calorimeter (ARC) to investigate the heat and gas release behaviour of HMX and PW/HMX between decomposition and thermal runaway.

Fig. 6a shows the heat release curves of HMX and PW/HMX under adiabatic conditions (data are summarized in Table S2†). It can be seen that HMX undergoes a self-sustaining decomposition at 499.7 K, and the heat generated from this process facilitates its further decomposition. At 511.5 K, HMX enters the thermal runaway state, and the rate of maximum temperature reaches 2960.7 K min^{-1}. The self-sustaining decomposition and thermal runaway for PW/HMX occur at 484.8 and 510.5 K, respectively, and the rate of maximum temperature rise rate is 1386.9 K min^{-1}. When no exothermic signal is detected, the pressures of PW/HMX and HMX are unchanged (Fig. 6b), and the pressure rise rates are also close to zero. After the self-sustaining decomposition, the pressure rise rate of PW/HMX increases rapidly, which is higher than that of HMX at the same temperature. The pressure of PW/HMX at thermal runaway is higher (190 kPa) than that of HMX (150 kPa) due to the rapid pressure rise rate, which implies that the decomposition of PW/HMX produces more gas. After the thermal runaway, the pressure rise rate of HMX increased rapidly, reaching 2540 kPa min^{-1}. This value for PW/HMX is only 950 kPa min^{-1}. The self-sustaining decomposition temperature for PW/HMX is 484.8 K, which is 14.9 K lower than that for HMX. However, this value is significantly higher than the initial temperature of the first decomposition process observed during the DSC test. This shows that although the decomposition of PW itself promotes the first decomposition process of HMX, the

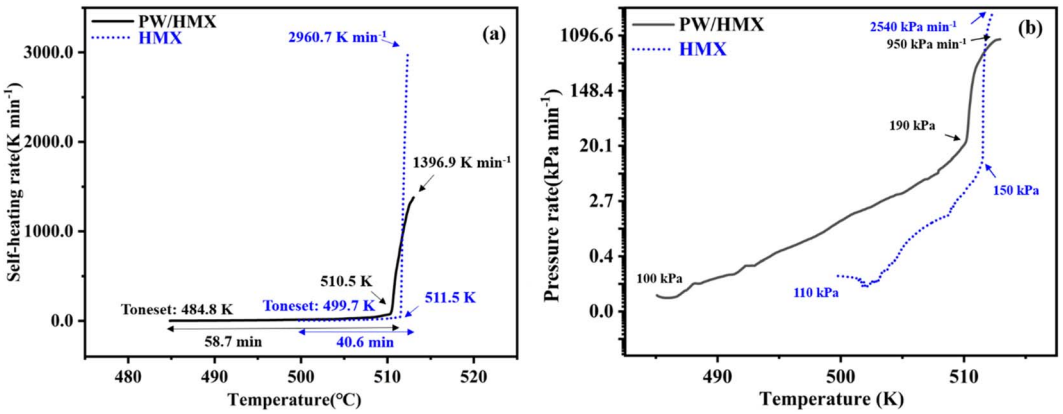

Fig. 6 Temperature increase rate as (a) and pressure increase rate (b) as a function of temperature.

heat release of PW does not cause HMX to enter into self-sustaining decomposition. The subsequent thermal runaway occurs at a temperature of 510.5 K and a pressure of 190 kPa, the former is almost the same as HMX, while the latter is higher than HMX. Although PW triggered the self-sustaining decomposition of HMX earlier, the thermal runaway was delayed by 18.1 min. This indicates that PW can not only induce the decomposition of HMX but also inhibit the transformation from decomposition to thermal runaway and reduce the reaction rate after the latter.

To further investigate the heat release processes, we fitted dynamic models to the results obtained for HMX and PW/HMX during adiabatic decomposition (further information is provided in the ESI†). The kinetic model of the adiabatic decomposition of HMX and PW/HMX is based on coupling the *n*-order and power-law autocatalytic models. The adiabatic decomposition curve reconstructed based on the kinetic model parameters is shown in Fig. S3.† The equation used is as follows:

$$\frac{da}{dt} = A(1-\alpha)^n(1+K_{cat}\alpha^m)e^{-\frac{E_a}{RT}}$$

where n is the reaction order, K_{cat} is the rate constant of autocatalytic kinetics, and m is the autocatalytic reaction order. The following kinetic parameters were calculated: the activation energy of HMX is 287.6 kJ mol^{-1}, the *n*-order reaction order was 0.3, K_{cat} is 0.6, and m is 10.0 (Table 1). Following the decomposition of PW/HMX, these values were 268.5 kJ mol^{-1}, 1.1, 0.28, and 2.3, respectively. These results indicate that compared with HMX, the dominant *n*-order reaction for PW/HMX increases at the initial stage of decomposition. As the reaction proceeds, the autocatalytic characteristic of the latter decreases, and PW inhibits the conversion of HMX from an *n*-order reaction to an autocatalytic reaction. In the PBX cylinder, this inhibition ability would allow the decomposition of more HMX, favouring more pre-damage before its ignition, further reducing energy release intensity during a slow cook-off.

3.4 Gas product analysis of self-sustaining decomposition

ARC-GC-MS was used to investigate the gaseous products formed during the decomposition of HMX and PW/HMX. The peak areas of gas products varied with the temperature, as shown in Fig. 7. Compared with HMX, the composition of gas products for PW/HMX did not change: they contained mainly N_2O, CO_2, N_2, NO, and CO. Without thermal runaway, the gases escaped, as expected, to a greater degree for PW/HMX than for HMX. However, as the decomposition progressed, the increase rate of gases for PW/HMX decreased gradually. For HMX, a steady increase was observed. This phenomenon can be related to the fact that PW induces the decomposition of HMX before the thermal runaway and reduces the reaction rate after the thermal runaway.

The relative content of active gas (NO) was also investigated with the decomposition of HMX and PW/HMX (Fig. 8). At the initial stage of the self-sustaining decomposition, the relative NO content in PW/HMX was significantly lower than that in HMX. As the decomposition progressed, the gap between them became smaller. NO formation can mainly be related to the degradation of $-NO_2$ groups in HMX.[32] Since PW promotes the first decomposition process of HMX, the content of NO in this process should be higher than that of pure HMX. However, the content of NO was actually lower than that of pure HMX, which indicated that PW not only promoted its decomposition but also accelerated the consumption of the generated active gas, leading to the reduction of the autocatalytic reaction effect.

Table 1 Kinetic fitting parameters of HMX and PW/HMX

Sample	Activation energy (kJ mol^{-1})	log(A) (S^{-1})	*N*-order reaction order	Autocatalytic kinetic rate constant	Autocatalytic reaction order	R^2
HMX	287.6	26.4	0.3	0.63	10.0	0.998
PW/HMX	268.5	22.6	1.1	0.28	2.3	0.999

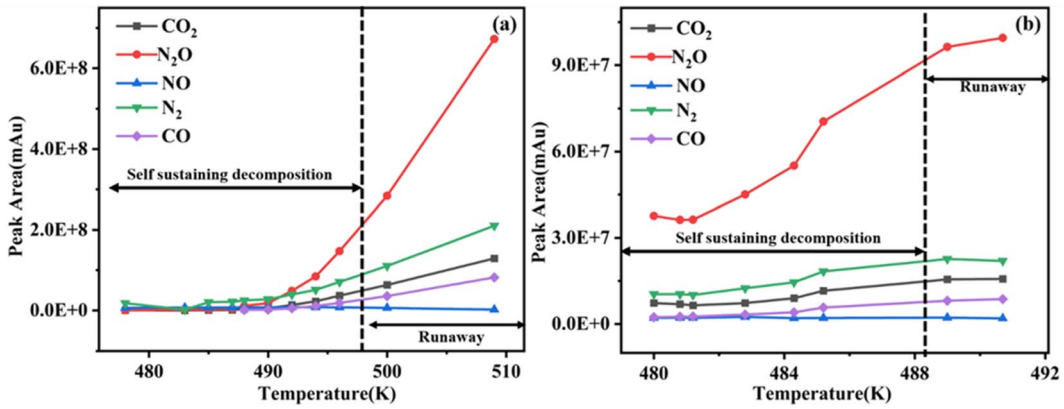

Fig. 7 Evolution of gas products as a function of time during the self-sustaining decomposition of (a) HMX and (b) PW/HMX.

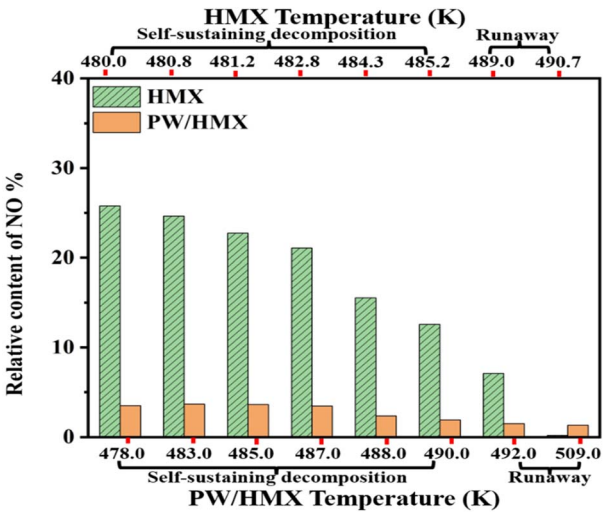

Fig. 8 Relative NO contents formed during the self-sustaining decomposition of HMX and PW/HMX.

4. Conclusions

PW and HMX have similar polarities. With the increase of temperature, PW can infiltrate the surface of HMX crystal after melting, thus reducing the chemical dissociation energy of surface molecules, resulting in the early decomposition of HMX surface molecules. Meanwhile, PW can consume the reaction gas produced by the reaction and reduce the reaction rate of HMX. In decomposition kinetic, PW inhibits the transformation of HMX from an *n*-order reaction to an autocatalytic reaction. These results show that PW has the potential to improve the thermal safety of HMX-based PBX.

Author contributions

Zunjian Hu: conceptualization, writing – original draft, writing – review and editing. Wei Peng: conceptualization, writing – original draft, writing – review and editing. Gang Li: writing – original draft, writing – review and editing. Fang Yang: writing – original draft, writing – review and editing. Qian Yu: writing – original draft, writing – review and editing. Zhirong Suo: writing – original draft, writing – review and editing. Ruijuan Xu: writing – original draft, writing – review and editing. Chuande Zhao: writing – original draft, writing – review and editing.

Conflicts of interest

There are no conflicts to declare.

Acknowledgements

We sincerely thank the Nature Science Foundation of China (No. 12002324, 12172342).

References

1 D. K. Rajak, D. D. Pagar, R. Kumar, C. Pruncu and R. I, *J. Mater. Res. Technol.*, 2019, **8**, 6354–6374.
2 M. C. Biswas, S. Chakraborty, A. Bhattacharjee and Z. Mohammed, *Adv. Funct. Mater.*, 2021, **31**, 2100257.
3 Y. Zhao, L. Hao, X. Zhang, S. Tan, H. Li, J. Zheng and G. Ji, *Small*, 2022, **2**, 2100077.
4 Q. L. Yan, M. Gozin, F. Q. Zhao, A. Cohen and S. P. Pang, *Nanoscale*, 2016, **8**, 4799–4851.
5 G. Li and C. Zhang, *J. Hazard. Mater.*, 2020, **398**, 122910.
6 Y. Xiao, Y. Sun, Y. Zhen, L. Guo and L. Yao, *Int. J. Impact Eng.*, 2017, **103**, 149–158.
7 X. Huang, Z. Huang, J. C. Lai, L. Li, G. C. Yang and C. H. Li, *Compos. Sci. Technol.*, 2018, **167**, 346–354.
8 R. G. Ewing, D. A. Atkinson, G. A. Eiceman and G. J. Ewing, *Talanta*, 2001, **54**, 515–529.
9 P. Chen, H. Xie, F. Huang, T. Huang and Y. Ding, *Polym. Test.*, 2006, **25**, 333–341.
10 G. X. Wang, H. M. Xiao, X. J. Xu and X. H. Ju, *Propellants, Explos., Pyrotech.*, 2006, **31**, 102–109.
11 X. Z. Yong, B. L. Da and X. L. Chun, *Propellants, Explos., Pyrotech.*, 2005, **30**, 438–441.
12 C. Y. Zhang, *J. Phys. Chem. C*, 2010, **114**, 5068–5072.
13 C. Lin, C. Zeng, Y. Wen, F. Gong, G. He, Y. Li and S. Guo, *ACS Appl. Mater. Interfaces*, 2019, **12**, 4002–4013.

14 S. A. Bordzilovskii and S. M. Karakhanov, *Combust., Explos. Shock Waves*, 1995, **31**, 227–235.
15 C. Zhang, Y. Li, Y. Xiong, X. Wang and M. Zhou, *J. Phys. Chem. A*, 2011, **115**, 11971–11978.
16 C. Zhao, Y. Chi, Q. Yu, X. Wang, G. Fan and K. Yu, *J. Phys. Chem. C*, 2019, **123**, 27286–27294.
17 R. De Avillez Pereira, D. L. Baulch, M. J. Pilling, S. H. Robertson and G. Zeng, *J. Phys. Chem. A*, 1997, **101**, 9681–9693.
18 B. Shanks, *Thermochim. Acta*, 2005, **148**, 365–373.
19 E. Salmon, A. C. van Duin, F. Lorant, P. M. Marquaire and W. A. Goddard III, *Org. Geochem.*, 2009, **40**, 1195–1209.
20 Q. D. Wang, X. X. Hua, X. M. Cheng, J. Li and X. Y. Li, *J. Phys. Chem. A*, 2012, **116**, 3794–3801.
21 A. K. Burnham, R. K. Weese and B. L. Weeks, *J. Phys. Chem. B*, 2004, **108**, 19432–19441.
22 C. Gao, L. Yang, Y. Zeng, X. Wang, C. Zhang, R. Dai and Z. Zhang, *J. Phys. Chem. C*, 2017, **121**, 17586–17594.
23 O. Sharia, R. Tsyshevsky and M. M. Kuklja, *J. Phys. Chem. Lett.*, 2013, **4**, 730–734.
24 T. Liu, C. Geng, B. Zheng, S. Li and G. Luo, *Propellants, Explos., Pyrotech.*, 2017, **42**, 1057–1065.
25 X. Li, J. Wang, W. Liu, C. Niu and C. Song, *Combust. Flame*, 2022, **240**, 111989.
26 Y. Kim, Y. Park and J. J. Yoh, *Thermochim. Acta*, 2019, **678**, 178300.
27 L. Chen, X. Ma, F. Lu and J. Wu, *Cent. Eur. J. Energetic Mater.*, 2014, **11**, 199–218.
28 X. Yan, X. D. Li, Y. R. Zhang, L. Liu, X. M. Zhang, Y. X. Tan and X. Q. Wang, *Cent. Eur. J. Energetic Mater.*, 2018, **15**, 339–350.
29 M. L. Gross, K. V. Meredith and M. W. Beckstead, *Combust. Flame*, 2015, **162**, 3307–3315.
30 Q. Ye and Y. G. Yu, *Appl. Therm. Eng.*, 2020, **181**, 115972.
31 L. X. Du, S. H. Jin, Q. H. Shu, L. J. Li, K. Chen, M. L. Chen and J. F. Wang, *Def. Technol.*, 2022, **18**, 72–80.
32 C. Zhao, Y. Chi, Q. Peng, F. Yang, J. Zhou, X. Wang and J. Sun, *Phys. Chem. Phys.*, 2019, **21**, 6600–6605.